

Sources of Error in a Rigid Body Simulation of Rigid Parts on a Vibrating Rigid Plate.

Stephen Berard
Rensselaer Polytechnic
Institute
110 8th Street
Troy, NY
sberard@cs.rpi.edu

Binh Nguyen
Rensselaer Polytechnic
Institute
110 8th Street
Troy, NY
nguyeb2@cs.rpi.edu

J.C. Trinkle
Rensselaer Polytechnic
Institute
110 8th Street
Troy, NY
trink@cs.rpi.edu

ABSTRACT

We present a simulation study of an important rigid body contact problem. The system in question is composed of a rigid plate and a single rigid body (or particle). The plate follows a prescribed periodic motion of small amplitude and high frequency, such that the net force applied to the part appears to be from a time-independent, position-dependent velocity field in the plane of the plate. Theoretical results obtained by Vose *et al.* were found to be in good agreement with simulation results obtained with the Stewart-Trinkle time-stepping method. In addition, simulations were found to agree with the qualitative experimental results of Vose *et al.* After such verification of the simulation method, additional numerical studies were done that would have been impossible to carry out analytically. Specifically, we were able to demonstrate the convergence of the method with decreasing step size (as predicted theoretically by Stewart). Further analytical and numerical studies will be carried out in the future to develop and select robust simulation methods that best satisfy the speed and accuracy requirements of different applications.

Categories and Subject Descriptors

I.6.4 [Simulation and Modeling]: Model Validation and Analysis

General Terms

Verification

Keywords

Simulation, Modeling, Complementarity Problem, Performance

1. INTRODUCTION

As in many other fields, simulation is becoming an increasingly important tool for supporting research in robotics. Not

surprisingly, many of the important problems that could yield closed-form analysis have been solved and studied thoroughly. Problems characterized by intermittent contact is one particularly important type of robotics problems for which research must rely on simulation techniques [3, 12, 7]. Evidence of the need for simulation is the recent trend of robotics researchers studying grasping, assembly, and dexterous manipulation problems using Open Dynamic Engine (ODE) [9]. ODE was developed for computer game applications, which has led its developers to trade physical accuracy for simulation speed and believable results. The fact is that researchers using ODE (hoping that it will work accurate enough for their particular problems) are constantly asking for more physically accurate simulation tool.

In this paper, we present initial results verifying the accuracy of the Stewart-Trinkle time-stepping method [11], which lies at the core of the dVC physics engine [1]. This method is derived directly from the instantaneous dynamic model written as dynamic complementarity problem [13] using Euler approximations of derivatives (described below) and including constraint stabilization terms. The resulting simulation method requires the solution of one complementarity problem per time step. One of the benefits of our time-stepper is that as the time step goes to zero, the solution trajectories converge to a solution of the original instantaneous-time problem [6, 10]. Additional results are presented showing the effects of various sources of model approximation errors. Most of the problems studied had time-stepping subproblems formulated as linear complementarity problems (LCPs). These were simulated using dVC. However, custom C-code was written for problem whose subproblems were formulated as nonlinear complementarity problems (NCPs). All the LCPs and NCPs were solved by the state-of-the-art complementarity solver, PATH [5].

All the results presented here were obtained through numerical studies of a challenging and important problem studied analytically and experimentally by Vose, Umbanhowar, and Lynch [15]. In particular, they studied the motion of a particle on a nominally rigid plate moving with a specified periodic (high frequency) trajectory. When viewed on a long time scale (several cycles at a time), such periodic inputs cause the friction forces to generate velocity fields that can be used to move parts along specified paths on the plate. This work is motivated by the problem of assembly of tiny parts that are very difficult for humans (or robots) to manipulate, but could possibly be assembled (possibly many at once) on a vibrating plate.

Permission to make digital or hard copies of all or part of this work for personal or classroom use is granted without fee provided that copies are not made or distributed for profit or commercial advantage and that copies bear this notice and the full citation on the first page. To copy otherwise, to republish, to post on servers or to redistribute to lists, requires prior specific permission and/or a fee.

SAC'09 March 8-12, 2009, Honolulu, Hawaii, U.S.A.

Copyright 2009 ACM 978-1-60558-166-8/09/03 ...\$5.00.

As will be seen below, the advantage of studying this problem via simulation is that after verifying our simulation results against their theoretical and (qualitative) experimental results, we were immediately able to study an extended array of problems that violated the assumptions made by Vose *et al.*, which were required for their analytical study. One of these assumptions was that the particle was always in sliding contact with the plate. It's main effect was to limit the location of the particle to a small region of the plate where the assumption held. We were able to study the motion of the particle in contact anywhere on the plate, observing motions with stick-slip behavior and loss of contact. In addition, we are able to study the effects of linear approximations of the friction cone, a commonly applied simplification of the dynamic model. Most of these results are discussed below. For additional details and numerical studies, see [2].

2. DYNAMIC MODEL

The system Vose, Umbanhowar, and Lynch studied [14, 15, 16] consists of two pieces (figure 1), a kinematically controlled plate and a dynamical part interacting with the plate. Let $\mathbf{q} = [x \ y \ z \ e_s \ e_x \ e_y \ e_z]^T$ be the configuration of the part

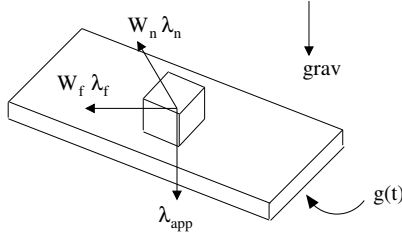


Figure 1: The plate is kinematically controlled by the function $g(t)$. There are three forces acting on the part: the force due to gravity λ_{app} , the non-penetration constraint force $\mathbf{W}_n \lambda_n$, and the frictional force $\mathbf{W}_f \lambda_f$.

where $[x \ y \ z]^T$ is the location of the center of gravity of the part in a fixed world frame and $[e_s \ e_x \ e_y \ e_z]^T$ is a unit quaternion representing the orientation of the part with respect to the fixed frame. $e_s = \cos(\theta/2)$ and $[e_x \ e_y \ e_z] = \sin(\theta/2)\mathbf{k}$ where θ is the angle of rotation and \mathbf{k} is the axis of rotation. Let $\mathbf{v} = [v_x \ v_y \ v_z \ \omega_x \ \omega_y \ \omega_z]$ be the velocity twist of the part, where \mathbf{v} is the translational velocity and $\boldsymbol{\omega}$ is the angular velocity. Let $\lambda_{\text{app}}(\mathbf{q}, t) \in \mathbb{R}^6$ represent the externally applied forces at time t , which for this problem is only gravity. Let $\lambda_{in} > 0$ be the magnitude of the normal contact force at the i th contact point, and λ_{it} and λ_{io} the corresponding orthogonal friction force components. Further, let λ_n be the concatenated vector of all the normal contact force magnitudes, and λ_t and λ_o the respective concatenated vectors for the tangential force magnitudes.

2.1 Discrete Time Dynamics

One natural way to model the dynamics of such a system with frictional intermittent contact is as a differential complementarity problem (DCP) [4, 8]. The details of the DCP formulation of the instantaneous dynamics for this system [14, 15, 16] can be found in [2]. However, the DCP is not solved directly, but instead a time-stepping scheme is employed and the resulting (possible nonlinear) mixed complementarity problem [4] is solved at each time step.

For completeness, we now present two velocity-level discrete time formulations of the instantaneous DCP: a nonlinear formulation and a linearized formulation. Let t_ℓ denote the current time and h be the time step. Use the superscripts ℓ and $\ell + 1$ to denote quantities at beginning and end of the ℓ th time step respectively.

2.1.1 NCP Formulation

Approximating $\dot{\mathbf{v}} \approx (\mathbf{v}^{\ell+1} - \mathbf{v}^\ell)/h$ and $\dot{\mathbf{q}} \approx (\mathbf{q}^{\ell+1} - \mathbf{q}^\ell)/h$, the nonlinear discrete time system can be written as:

$$\mathbf{M}\mathbf{v}^{\ell+1} = \mathbf{M}\mathbf{v}^\ell + h(\mathbf{W}_n \lambda_n^{\ell+1} + \mathbf{W}_t \lambda_t^{\ell+1} + \mathbf{W}_o \lambda_o^{\ell+1} + \lambda_{\text{app}}^\ell + \lambda_{\text{vp}}^\ell) \quad (1)$$

$$\mathbf{q}^{\ell+1} = \mathbf{q}^\ell + h\mathbf{G}\mathbf{v}^{\ell+1} \quad (2)$$

$$0 \leq \lambda_n^{\ell+1} \perp \psi_n(\mathbf{q}^{\ell+1}) \geq 0 \quad (3)$$

$$0 = (\mathbf{U}\lambda_n^{\ell+1}) \circ (\mathbf{v}_t^{\ell+1}) + \lambda_t^{\ell+1} \circ \boldsymbol{\sigma}^{\ell+1} \quad (4)$$

$$0 = (\mathbf{U}\lambda_n^{\ell+1}) \circ (\mathbf{v}_o^{\ell+1}) + \lambda_o^{\ell+1} \circ \boldsymbol{\sigma}^{\ell+1} \quad (5)$$

$$0 \leq \boldsymbol{\sigma}^{\ell+1} \perp (\mathbf{U}\lambda_n^{\ell+1}) \circ (\mathbf{U}\lambda_n^{\ell+1}) - \lambda_t^{\ell+1} \circ \lambda_t^{\ell+1} - \lambda_o^{\ell+1} \circ \lambda_o^{\ell+1} \geq 0 \quad (6)$$

Equation (1) is the Newton-Euler equations of the system.

The matrix $\mathbf{M}(\mathbf{q}^\ell) = \begin{bmatrix} m\mathbf{I}_{3 \times 3} & 0 \\ 0 & \mathcal{I}(\mathbf{q}^\ell) \end{bmatrix}$ is the mass-inertia matrix of the part, where m is the mass of the part and \mathcal{I} is the inertia tensor. The vector $\lambda_{\text{vp}} = \begin{bmatrix} 0 \\ -\boldsymbol{\omega}^\ell \times \mathcal{I}(\mathbf{q}^\ell)\boldsymbol{\omega}^\ell \end{bmatrix}$ is the velocity product term of Euler's equation. The matrices $\mathbf{W}_{(\cdot)} = [\dots \mathbf{W}_{i(\cdot)} \dots] \in \mathbb{R}^{6 \times n_c}$, where n_c is the number of contacts, are dependent on \mathbf{q} and map the normal and frictional wrench magnitudes to the body reference frame.

Equation (2) is the kinematic map of the system where \mathbf{G} is the matrix mapping the generalized velocity of the body to the time derivative of the position and orientation. $\mathbf{G}(\mathbf{q}^\ell) = \begin{bmatrix} \mathbf{I}_{3 \times 3} & 0_{3 \times 3} \\ 0_{4 \times 3} & \mathbf{J}_{4 \times 3}(\mathbf{q}^\ell) \end{bmatrix}$ where $\mathbf{I}_{3 \times 3}$ is the identity matrix of given

$$\text{size and } \mathbf{J}(\mathbf{q}^\ell) = \frac{1}{2} \begin{bmatrix} -e_x & -e_y & -e_z \\ e_s & e_z & -e_y \\ -e_z & e_s & e_x \\ e_y & -e_x & e_s \end{bmatrix}.$$

Equation (3) is the nonpenetration constraint for all contacts written as a complementarity condition where ψ_n is a concatenated vector of all the signed distance functions for each contact i (*e.g.* the signed distance between the part's corners and the kinematic plate's face). The distance is positive at contact i when the vertex-face pair at this contact is separated, it becomes zero when the vertex-face pair is touching, and it becomes negative when the vertex has penetrated the face. Note that in general there is no closed form expression for $\psi_{in}(\mathbf{q}, t)$ and it is approximated as, $\psi_{in}(\mathbf{q}^{\ell+1}, t_{\ell+1}) \approx \psi_{in}(\mathbf{q}^\ell, t_{\ell+1}) + h\mathbf{W}_{in}^T \mathbf{v}^{\ell+1}$. The notation $\psi_{in}(\mathbf{q}^\ell, t_{\ell+1})$ is used to indicate that the collision detection is done with the part at time t_ℓ and the plate at time $t_{\ell+1}$. This is possible because the kinematically controlled plate has a known function of time. This allows for the only approximation in the gap function to be the motion of the part. If we evaluate $\mathbf{W}_{(\cdot)}$ at $\ell + 1$, we have a fully implicit formulation [3] with an approximation in the gap function. If we evaluate $\mathbf{W}_{(\cdot)}$ at ℓ , we recover the Stewart-Trinkle formulation [11] with quadratic friction law.

Equations (4)–(6) represent Coulomb's friction law, writ-

ten compactly for all contacts, where \mathbf{U} is a diagonal matrix with i^{th} diagonal element equal to μ_i , the coefficient of friction (in this paper, the kinetic and static coefficients of friction are equal, so no distinction is made) at contact i , σ_i is a Lagrange multiplier arising from the conversion of the maximum dissipation condition from its ‘‘argmax’’ form into the inequality form given above, \mathbf{v}_t and \mathbf{v}_o are the concatenated vectors of sliding velocities for all contacts, and \circ connotes the Hadamard product (*i.e.* $\mathbf{a} \circ \mathbf{b} = [a_1 b_1 \ a_2 b_2 \ \dots \ a_n b_n]^T$). The value of σ_i also has a physical interpretation, it is the sliding speed at contact i .

The orthogonal sliding velocity components v_{it} and v_{io} for this system with a kinematically controlled plate can be written as:

$$v_{it} = \mathbf{W}_{it}^T(\mathbf{q})\boldsymbol{\nu} - \mathbf{W}_{it}^T(g)\mathbf{G}^T(g) \left(\frac{\partial g}{\partial t} \right)^T \quad (7)$$

$$v_{io} = \mathbf{W}_{io}^T(\mathbf{q})\boldsymbol{\nu} - \mathbf{W}_{io}^T(g)\mathbf{G}^T(g) \left(\frac{\partial g}{\partial t} \right)^T \quad (8)$$

where $g(t) : \mathbb{R} \rightarrow \mathbb{R}^7$ is the vector function providing the position and orientation (unit quaternion) of the plate at time t .

2.1.2 LCP Formulation

In order to obtain a scheme based on mixed LCPs [11], a piecewise linear approximation of the quadratic friction cone with nonnegative force variables is needed (figure 2). For completeness, we present the derivation below.

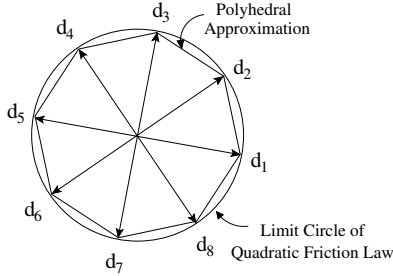


Figure 2: Friction cone approximated by an eight-sided pyramid defined by friction direction vectors \mathbf{d}_j .

Let n_d friction force direction vectors \mathbf{d}_j be chosen such that they positively span the space of possible friction forces, and let $(\lambda_{if})_j$ be the friction force components in those directions. Let $\mathbf{W}_f = [\dots \ \mathbf{W}_{if} \ \dots]$ where

$$\mathbf{W}_{if} = \begin{bmatrix} \mathbf{d}_1 & \dots & \mathbf{d}_{n_d} \\ \mathbf{r}_i \times \mathbf{d}_1 & \dots & \mathbf{r}_i \times \mathbf{d}_{n_d} \end{bmatrix}$$

Define orthogonal sliding velocity component

$$(v_{if})_j = (\mathbf{W}_{if})_j^T \boldsymbol{\nu} + (\mathbf{W}_{ikf})_j^T \mathbf{G}^T \left(\frac{\partial g}{\partial t} \right)^T \quad (9)$$

where $\mathbf{W}_{ikf} = \begin{bmatrix} -\mathbf{d}_1 & \dots & -\mathbf{d}_{n_d} \\ \mathbf{s}_i \times -\mathbf{d}_1 & \dots & \mathbf{s}_i \times -\mathbf{d}_{n_d} \end{bmatrix}$.

The maximum dissipation law for contact i can now be written

$$0 \leq (\lambda_{if})_j \perp (v_{if})_j + \sigma_i \geq 0, \quad j = 1 \dots n_d \quad (10)$$

$$0 \leq \sigma_i \perp \mu_i \lambda_{in} - \mathbf{e}^T \boldsymbol{\lambda}_{if} \geq 0 \quad (11)$$

where $\mathbf{e} \in \mathbb{R}^{n_d}$ is a vector of ones.

The maximum dissipation for all contacts can be written compactly as:

$$0 \leq \boldsymbol{\lambda}_f \perp \mathbf{v}_f + \mathbf{E}\boldsymbol{\sigma} \geq 0 \quad (12)$$

$$0 \leq \boldsymbol{\sigma} \perp \mathbf{U}\boldsymbol{\lambda}_n - \mathbf{E}^T \boldsymbol{\lambda}_f \geq 0 \quad (13)$$

where \mathbf{U} is a diagonal matrix with i^{th} element equal to μ_i and \mathbf{E} is a block diagonal matrix with i^{th} block on the main diagonal given by \mathbf{e} . Now σ_i approximates the sliding speed at contact i .

Putting it all together, we arrive at the following mixed LCP formulation:

$$\begin{aligned} \mathbf{M}\boldsymbol{\nu}^{\ell+1} &= \mathbf{M}\boldsymbol{\nu}^\ell + h(\mathbf{W}_n\boldsymbol{\lambda}_n^{\ell+1} + \mathbf{W}_f\boldsymbol{\lambda}_f^{\ell+1} + \boldsymbol{\lambda}_{\text{app}}^\ell + \boldsymbol{\lambda}_{\text{vp}}^\ell) \\ \mathbf{q}^{\ell+1} &= \mathbf{q}^\ell + h\mathbf{G}\boldsymbol{\nu}^{\ell+1} \\ 0 &\leq \boldsymbol{\lambda}_n^{\ell+1} \perp \psi_n(\mathbf{q}^{\ell+1}) \geq 0 \\ 0 &\leq \boldsymbol{\lambda}_f^{\ell+1} \perp \mathbf{v}_f^{\ell+1} + \mathbf{E}\boldsymbol{\sigma}^{\ell+1} \geq 0 \\ 0 &\leq \boldsymbol{\sigma}^{\ell+1} \perp \mathbf{U}\boldsymbol{\lambda}_n^{\ell+1} - \mathbf{E}^T \boldsymbol{\lambda}_f^{\ell+1} \geq 0 \end{aligned} \quad (14)$$

where $\psi_{in}(\mathbf{q}^{\ell+1}, t_{\ell+1}) \approx \psi_{in}(\mathbf{q}^\ell, t_{\ell+1}) + h\mathbf{W}_{in}^T \boldsymbol{\nu}^{\ell+1}$.

3. RESULTS

In this section we present various results of our simulations. The first set of results compares the simulated motion of a particle to its theoretically predicted motion. The next set of results compares the trajectory error as a function of friction cone approximation. Finally, we present results on the solution time of the underlying complementarity problem. The affects of step size and other details are given in [2].

3.1 Simulation Verification

In this section, we show that the results of simulation using the Stewart-Trinkle time-stepper agree with the analytical results obtained by Vose *et al.* They were able to obtain closed-form solutions of particle motion for a given a 2D version of the system (shown in Figure 3). In this system, the plate oscillates about an axis parallel to the plate’s surface and d units below it. While a block is shown in the figure, the analysis was only for a particle. Similarly, the simulation results presented in this section were obtained with a particle body. In [14], Vose *et al.* showed that particles converge to a unique velocity for each position r on the plate, which they call the asymptotic velocity at r .

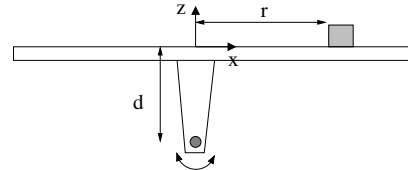


Figure 3: A part on a plate rotating about an axis below the plate. The fixed world frame is centered on the plate.

The particular plate motion analyzed in their paper is given by the following control function. Let $\theta(t)$ be the angle

of the plate at time t with period T defined by:

$$\theta(t) = \begin{cases} \frac{1}{2}\alpha t^2 - \frac{1}{4}\alpha T t & \text{if } 0 \leq t < T/2, \\ -\frac{1}{2}\alpha t^2 + \frac{3}{4}\alpha T t - \frac{1}{4}\alpha T^2 & \text{if } T/2 \leq t < T \end{cases} \quad (15)$$

Vose *et al.* impose two restrictions in order to obtain a solution for the asymptotic velocity of the particle, it never loses contact with the plate and it never sticks to the plate. Under these assumptions, the average horizontal asymptotic velocity of the part v_{ss} can be computed as

$$v_{ss} = br + cr^3 \quad (16)$$

where b and c are constants defined in their paper.

The first test we performed was a comparison between their numerically computed asymptotic velocity of the part and the asymptotic velocity of the part found in our simulation. To compute the asymptotic velocity, we recorded the average velocity of the particle for each period of the plate's motion. Since the particle does not move very far in a single period of the plate's motion, we consider this average velocity an estimate of the asymptotic velocity. In addition, we also computed the average position of the particle (in the plate's frame) and used the x component of the average position in equation (16). In order to satisfy the required assumptions of their analysis, we set $\alpha = 180$, the period $T = .03$ seconds, and placed the axis of rotation 5cm below the plate.

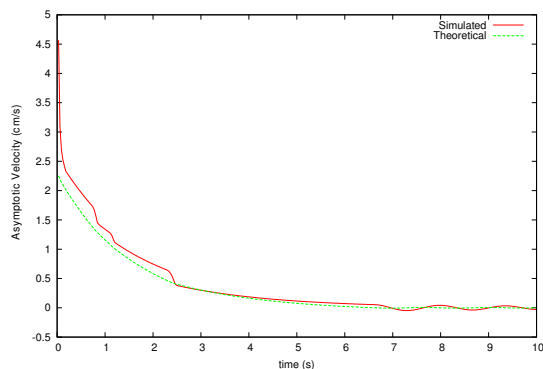


Figure 4: Comparison between the numerically computed asymptotic velocity (simulated) to the value determined in the work of Vose *et al.* (theoretical).

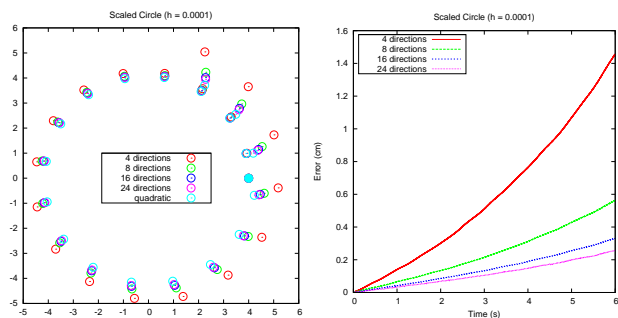
Figure 4 illustrates a comparison between the numerically computed horizontal asymptotic velocity determined in the work of Vose *et al.* to our simulated velocity. Note that initially the simulation velocity is much larger than the predicted steady state velocity, but over time, the particle's velocity appears to converge to the steady state velocity. This result suggests that our time-stepping method gives a faithful representation of the dynamic model of the system. A second indication that our simulation method was producing correct results was done by qualitative comparison of our simulations with those produced by Vose *et al.* Our simulator qualitatively matched the results they published in [14, 15] and observations of their experimental system.

One last point of comparison of analytical and simulated results was obtained by varying the problem parameters. By simply moving the axis of rotation closer to the plate, our simulation and the experimental results of Vose *et al.*

show that particle sticks during portions of each cycle of the plate's motion. This violates the assumptions used in the analysis and thus analytical prediction of particle steady-state motion for this case is invalid.

3.2 Trajectory Error as a Function of Friction Cone linearization

In this section, we look at how the trajectory of the part on the plate varies as a function of the friction linearization level used in the discretized mixed complementarity problem formulation. We use the same part model as in the previous section, but now keep the step size constant (at $h = 0.0001$ seconds) and use a (regular) polyhedral approximation of the friction law at each tripod support point. The trajectories are parameterized by the number of edges in the polyhedral approximation. A baseline trajectory is computed by using the quadratic form of Coulomb's law at the contact point. Taking this trajectory as "correct", the error in the other trajectories is the distance at time t from the base trajectory at time t .



(a) Trajectory (ticks placed at 0.3 second intervals) (b) Trajectory Error

Figure 5: Trajectory and error caused by the polygonal approximation of the friction code. The error at time t is the Euclidean distance of the particle between the LCP and NCP formulations. The initial position of the particle was (4,0) and all simulations used a step size of 0.0001 seconds.

The results in figure 5 are for a scaled version of the Circle motion described in [15]. For the scaled circle we scaled the angular acceleration by a factor of 5, resulting in the following plate motion function:

$$\alpha_z = 5(100 \sin(66\pi t)) \quad (17)$$

$$\ddot{p}_z = 8 \sin\left(66\pi t + \frac{3}{2}\pi\right) \quad (18)$$

With the plate subject to the scaled circle trajectory (figure 5a), increasing the number of friction directions increasingly improves the trajectory error (figure 5b).

3.3 Solution Time of Problem

Another consideration of analysis by simulation is the computation time. For example, the 5 second simulation of the scaled circle field controller using the LCP formulation with 3 contacts and 32 friction directions took slightly over 2 minutes to complete on a standard laptop (Intel Pentium M processor 1.60GHz). Conversely, the "harder" nonlinear complementarity problem formulation with quadratic friction law took a little over 20 seconds to complete.

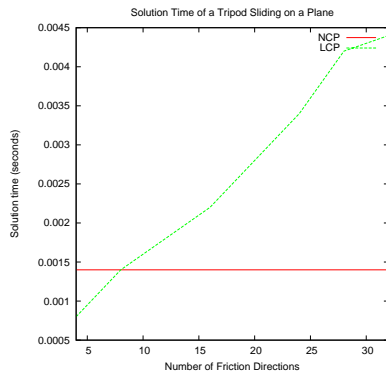


Figure 6: Timing of a single LCP function call for a block sliding on a plane as a function of number of friction directions. The solution time for an equivalent NCP formulation with quadratic friction law is also plotted. At approximately 8 friction directions, the solution time of the LCP is larger than the NCP.

The above results indicate that the NCP formulation is not only more accurate, but also significantly faster than the the LCP formulation for reasonable levels of friction cone linearization accuracy. The solution time of a single LCP (using the PATH solver) for various levels of friction approximation is shown in figure 6. The size of the LCP is $12 + 3d$, where d is the number of friction directions. For comparison, the solution time of the equivalent NCP is also plotted. At approximately 8 friction directions, the solution time of the LCP is larger than the NCP. This is an important finding given that for all the above simulations, 8 friction directions is insufficient for generating accurate simulations.

4. CONCLUSION AND FUTURE WORK

In this paper, we discussed simulation results for rigid bodies in intermittent frictional contact with a rigid plate undergoing a prescribed spatial trajectory, as studied theoretically and experimentally by Vose, Umbanhowar, and Lynch [15]. The results were obtained with a complementarity based time-stepping method whose subproblems were formulated as complementarity problems. It was verified that the simulation method matched the theoretical results and agreed qualitatively with simulations of problems for which only qualitative experimental results were available.

After verifying our code in this manner, we studied the convergence behavior of part trajectories as a function of friction cone linearization and found that the NCP formulation is not only more accurate, but also significantly faster than the the LCP formulation for reasonable levels of friction cone linearization accuracy.

In future work, we plan to study other sources of error and quantify their impact on simulation accuracy. This will lead to methods for developing adaptive step size selection for controlling simulation error. In fact, this work will go even further. We will gain a thorough understanding of errors caused by linearization of the friction cones, body geometry, and distance functions. Ultimately, we plan to develop a method that adaptively makes model linearization decisions to bound errors from those sources with an acceptable

solution time.

5. REFERENCES

- [1] S. Berard, B. Nguyen, B. Roghani, J. Trinkle, J. Fink, and V. Kumar. daVinci Code: A multi-model simulation and analysis tool for multi-body systems. In *IEEE ICRA*, 2007.
- [2] S. Berard, B. Nguyen, and J. C. Trinkle. Sources of error in a rigid body simulation of rigid parts on a vibrating rigid plate. Technical Report 08-10, Department of Computer Science, Rensselaer Polytechnic Institute, 2008.
- [3] N. Chakraborty, S. Berard, S. Akella, and J. Trinkle. An implicit time-stepping method for multibody systems with intermittent contact. In *Robotics: Science and Systems*, June 2007.
- [4] R. W. Cottle, J. Pang, and R. E. Stone. *The Linear Complementarity Problem*. Academic Press, 1992.
- [5] M. C. Ferris and T. S. Munson. Complementarity problems in GAMS and the PATH solver. *Journal of Economic Dynamics and Control*, 24(2):165–188, 2000.
- [6] B. Gavrea, M. Anitescu, and F. Potra. Convergence of a class of semi-implicit time-stepping schemes for nonsmooth rigid multibody dynamics. *SIAM Journal on Optimization*, To Appear.
- [7] E. Johnson and T. Murphey. Discrete and continuous mechanics for tree representations of mechanical systems. In *IEEE International Conference on Robotics and Automation*, 2008.
- [8] J.-S. Pang and F. Facchinei. *Finite-Dimensional Variational Inequalities and complementarity Problems (I)*. Springer Verlag, New York, 2003.
- [9] R. Smith. Open dynamics engine, 2008. <http://www.ode.org>.
- [10] D. Stewart. Convergence of a time-stepping scheme for rigid-body dynamics and resolution of Painlevé’s problem. *Archive for Rational Mechanics and Analysis*, 145(3):215–260, 1998.
- [11] D. Stewart and J. Trinkle. An implicit time-stepping scheme for rigid body dynamics with inelastic collisions and coulomb friction. *Int’l Jnl. of Numerical Methods in Engineering*, 39:2673–2691, 1996.
- [12] S. Sueda, A. Kaufman, and D. K. Pai. Musculotendon simulation for hand animation. *ACM Trans. Graph. (Proc. SIGGRAPH)*, 27(3), 2008.
- [13] J. Trinkle, J. Pang, S. Sudarsky, and G. Lo. On dynamic multi-rigid-body contact problems with Coulomb friction. *Zeitschrift für Angewandte Mathematik und Mechanik*, 77(4):267–279, 1997.
- [14] T. H. Vose, P. Umbanhowar, and K. M. Lynch. Vibration-induced frictional force fields on a rigid plate. In *IEEE International Conference on Robotics and Automation*, 2007.
- [15] T. H. Vose, P. Umbanhowar, and K. M. Lynch. Friction-induced velocity fields for point parts sliding on a rigid oscillated plate. In *Robotics: Science and Systems*, 2008.
- [16] T. H. Vose, P. Umbanhowar, and K. M. Lynch. Friction-induced lines of attraction and repulsion for parts sliding on an oscillated plate. *IEEE Transactions on Automation Science and Engineering*, To Appear.